Multiple electron capture spectroscopy

Unipan, Mirko

CHAPTER

SIX

He^{**} MECS: fundamentals and application to Ni(110)

In this chapter we will focus on a detailed description of the model used to analyze and explain the results of chapter 5, and show new experimental results. In MECS, the changes in the characteristic Auger electron emission from doubly-excited He atoms are used as a fingerprint of the local surface spin polarization. The He^{**} atoms are formed upon neutralization of He^{2+} ions in front of a surface, in this case ferromagnetic Ni(110), by resonant capture of two electrons from the surface into atomic levels.

The neutralization of slow, multiply charged ions in front of surfaces can be described by the classical over-the-barrier (COB) model [16]. According to the COB model, resonant electron capture from the metal becomes possible at a distance where the potential barrier between the solid and the ion is lowered to the Fermi level. The electrons are captured into high-lying shells of the projectile, which can subsequently de-excite by auto-ionization. The emitted Auger electrons produce characteristic electron-energy spectra [16–20]. While the ion further approaches the surface, an interplay between electron loss to the solid (reionization) and electron capture from the surface takes place. The energy distribution of the emitted electrons contains information on the neutralization process and on the electronic structure of the surface [14, 38, 89]. For example, the dynamic response of the solid influences the shape of the Auger electron spectra, the peak positions in the KLL Auger spectra from He^{**} being shifted to higher

energies as compared to emission from gas phase atoms [38]. Also, from the evolution of the spectra with projectile energy information on the magnitude of the resonant ionization rate can be obtained.

As the spin of the electrons is conserved in the capture process [1, 7], there will be different capture probabilities for different spin states if the surface is spin-polarized, i.e., majority and minority electrons having different densities of states close to the Fermi level. If the surface has a high degree of spin polarization, it will be more probable to capture electrons into high spin states (in the case of He, triplet states), while for a low surface polarization, low spin states (singlet states for He) are favoured. When the doubly excited He atoms relax by Auger processes, the relative peak intensities in the KLL Auger spectra (corresponding to triplet or singlet states) will change if the surface spin polarization changes, e.g., by changing the temperature of a ferromagnet (as shown in the previous chapter). As slow He^{2+} ions interact only with an area of a few (tens of) $Å^2$ of the top-most surface layer, MECS has the potential of becoming an useful tool for studying surface magnetism, yielding complementary information to other techniques which can probe magnetism on a scale below the exchange length, like spin-polarized STM [61].

6.1 Free-atom model

In this section we outline the model which we propose for the description of KLL Auger electron spectra from He^{2+} ions scattering off a ferromagnetic surface, in our case a Ni(110) surface. In this so-called 'free-atom model', the $(2l2l')$ states in doubly excited He are allowed to decay exponentially like in free atoms, and it is assumed that the auto-ionization rates do not change as the projectile approaches the surface. Besides electron emission by auto-ionization (AI), electron loss to the solid by resonant ionization (RI) is also taken into account. The influence of the surface spin polarization on the capture probability for different states in He^{**} is incorporated, which, in turn, influences the shape of KLL Auger spectra from He^{**}.

The relevant states in doubly excited He, which are the initial states in the auto-ionization processes, are listed in Table 6.1. The kinetic energy ε_k of an Auger electron is given by the difference in binding energy E_{bin} between the initial $(2l2l')$ state in He^{**} and the final He^+ $(1s)$ state (which has a binding energy of 54.42 eV). The auto-ionization rates listed in Table 6.1 are values calculated by Lindroth [86] for free He^{**} atoms. Other calculated [90,91] and experimental [92] AI rates have similar values. For the $(2s2p)$ ^{3}P state no experimental AI rate is available, only an upper limit of $0.23 \cdot 10^{14}$ s^{-1} has been determined [92]. The decay from the $(2p^2)$ ^{3}P state is forbidden, while the rate for the $(2p^2)$ ^{1}S is very small. Therefore, only four states contribute to the auto-ionization spectra from

Table 6.1: *Electronic configurations, statistical weights g, binding energies (E_{bin}), Auger electron energies (ε_k), and auto-ionization rates (Γ_{AI}) [86] for doubly excited $He^{**}(2l2l')$.*

State	g	E_{bin} [eV]	ε_k [eV]	Γ_{AI} [10^{14} s^{-1}]
$(2s^2)\ ^1S$	1	21.13	33.3	1.87
$(2s2p)\ ^3P$	9	20.69	33.7	0.12
$(2p^2)\ ^3P$	9	19.33	-	0
$(2p^2)\ ^1D$	5	19.12	35.3	0.95
$(2s2p)\ ^1P$	3	18.88	35.5	0.54
$(2p^2)\ ^1S$	1	16.86	37.3	$\ll 0.01$

He^{**}, namely $(2s^2)\ ^1S$, $(2s2p)\ ^3P$, $(2p^2)\ ^1D$ and $(2s2p)\ ^1P$.

6.1.1 Features of the ion-surface interaction in KLL Auger spectra from He^{**}

In our model we assume that the He^{**} atoms are formed at a distance in front of the surface where resonant over-the-barrier transitions become possible. According to the classical over-the-barrier model [16], the neutralization distance of He^{+*} is about 8 a.u. (eq. 2.3), for the typical workfunction of metals of ~ 5 eV. Once neutralized, the excited atom will decay by auto-ionization as it approaches the surface. Close in become the main de-excitation mechanisms, by which the atomic levels are quenched. The presence of the surface strongly atomic levels are quenched. The presence of the surface strongly perturbs the atomic levels.

The electrons originating from Auger de-excitation or Auger neutralization processes are not taken into account in our model, as they give a broad distribution at lower energies, the higher-energy tail of these electrons being treated as background to the AI signal (cf. Fig. 5.1). Elastically scattered auto-ionization electrons could end up in the atomic lines, but as only the energy of the electrons is detected as a measure of the initial state from which they originate, the small spin-flip probability [93] of these electrons has no influence on the analysis. The inelastically scattered auto-ionization electrons will show up at lower energies largely outside the atomic lines.

The atomic levels into which the surface electrons are captured shift in energy depending on the ion-surface distance z, owing to the charge - image charge Coulomb interaction. For the atomic charge an "effective' charge is taken, which accounts for the incomplete screening of the nuclear charge by the electronic cloud. The effective charge is also z-dependent. For the doubly-excited He atoms

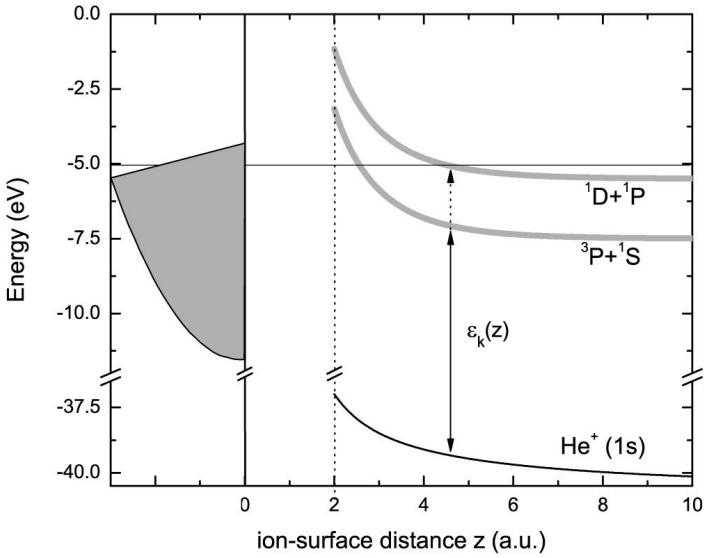

Figure 6.1: *Illustration of the different level shifts for the* $(2l2l')$ *states in He*** *compared to the* $(1s)$ *state in He*$^+$.

the effective charge is taken as $Z_{eff}(z) = 2e^{-z/3.5}$, while for He^+ it is taken as $Z_{eff}(z) = 1 + e^{-z/0.72}$ [38]. The atomic levels shift in energy as $Z^2_{eff}/4z$. The potential curves for the initial $(2l2l')$ states in He^{**} have then a different energy shift as compared to the one for the final He^+ $(1s)$ state. As the energy difference between the potential energy curves of the initial and final states is z-dependent, the energy of the atomic Auger transitions will change as the projectile approaches the surface, as illustrated in Fig 6.1. In addition, in order to take the dynamic response of the metal into account, the final energy of the auto-ionization electron $\varepsilon_k(z)$ is taken in between two extreme cases, i.e. the adiabatic and the diabatic case. The adiabatic case corresponds to an infinitely fast rearrangement of the metal electrons, while the diabatic case corresponds to an infinitely slow rearrangement. The ratio between the velocity of the emitted electrons and the Fermi velocity of the metal, $\rho = v_a/v_F$, can be regarded as the fastness of the response of the solid to the ionization event. Zeijlmans van Emmichoven *et al.* [38] proposed the following expression for the transition energy:

$$\varepsilon_k(z) = \varepsilon^d_k(z) + (\varepsilon^a_k(z) - \varepsilon^d_k(z))e^{-\rho/2} \tag{6.1}$$

where ε^d_k and ε^a_k are the energies of the auto-ionization electron for the diabatic and the adiabatic case, respectively. For the case of the Ni(110) surface and the typical energies of the He^{**} auto-ionization electrons, $\rho \simeq 2$. Therefore, the energies ε^d_k and ε^a_k differ by about 0.5 eV, as calculated from eq. 2.19.

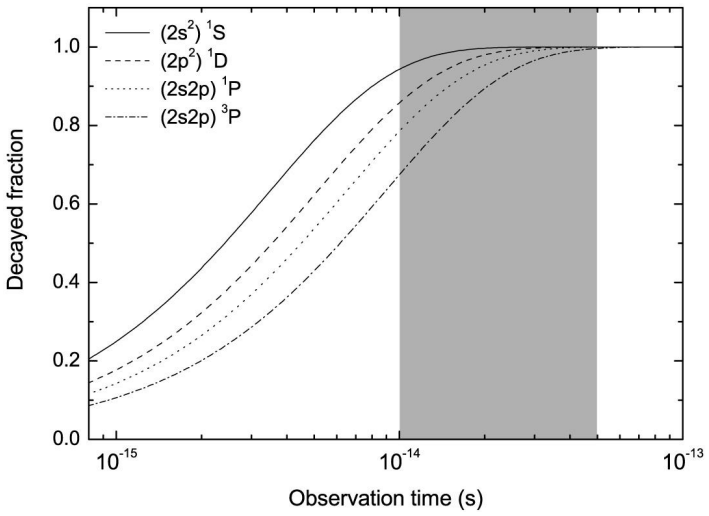

Figure 6.2: *Fractions decayed by AI for the four relevant* $(2l2l')$ *states in He**. Typical observation times from our experiments are indicated by the shaded area.*

Fig. 6.1 shows schematically the shift of the four relevant atomic levels in doubly excited He relative to the electronic structure of the Ni(110) surface. The density of states for Ni(110) is shown here as a modified free-electron metal DOS. This kinematically shifted DOS is the DOS seen in the reference frame of the moving ion (here shown for illustration for an ion velocity of 0.05 a.u.) [35, 43, 44]. The relevant atomic levels are below the Fermi energy (which is 5.05 eV below vacuum and 9.1 eV above the bottom of the conduction band in the case of Ni(110) [69]) for almost all atom-surface distances. This allows for resonant capture of electrons into these states as soon as the potential barrier between the projectile and the surface is low enough. Due to the parallel velocity of the incoming projectile, the electrons of the solid are seen by the ion as having an apparent lower work function, because of the kinematically shifted DOS [35, 43, 44]. Therefore electron capture is possible even if the atomic levels are shifted above the 'static' Fermi energy.

After resonant electron capture into the He** states, the part of the initial population which has decayed by AI in the time t is given by:

$$I_{if}(t) = g_i \Gamma^{if} \tau_i (1 - e^{-t/\tau_i}) \tag{6.2}$$

where g_i is the statistical weight of the state i, Γ^{if} is the decay rate of the specific $i \rightarrow f$ transition and $\tau_i = (\Gamma^{if}_{AI} + \Gamma_{RI})^{-1}$ is the lifetime of state i. Decay by resonant ionization was included with an estimated rate of $\Gamma_{RI} = 10^{15}$ s^{-1} [94]. The auto-ionization rates Γ^{if}_{AI} (taken from Table 6.1) and the resonant ionization

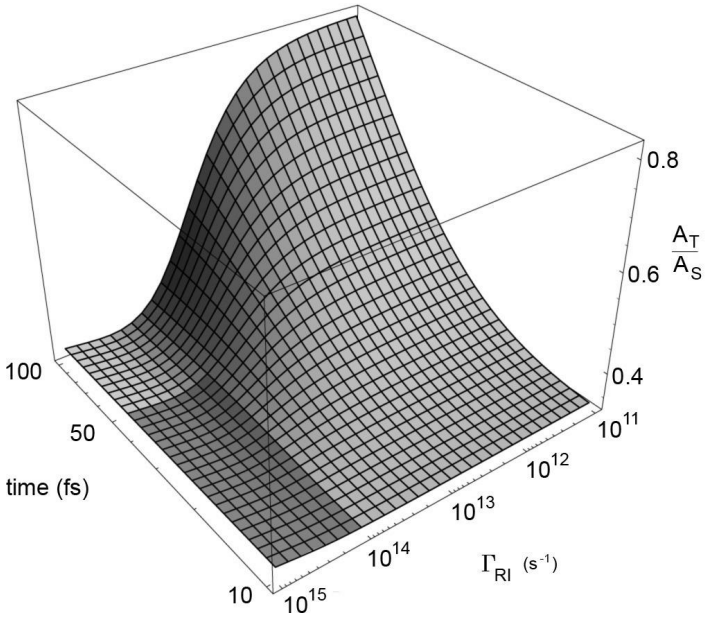

Figure 6.3: *Triplet-to-singlet peak ratio for an unpolarized surface.*

rate Γ_{RI} are assumed not to depend on the ion-surface distance z within the relevant range of z-values. The normalized decayed fractions $(I_{if}(t)/g_i)$ for the four states in He** are shown in Fig. 6.2. By summing the decayed fractions $I_{if}(t)$ for the two pairs of states in He**, the triplet-to-singlet intensity ratio A_T/A_S is obtained. For the decay of the He** atoms by AI, only the time between neutralization and quenching of the atomic states at the surface is available [16,38,81]. For our experiments, this time is in the interval $10-50$ fs (indicated by the shaded area in Fig. 6.2). In Fig. 6.3 the triplet-to-singlet peak ratio A_T/A_S is shown as function of the resonant ionization rate and observation time, for an unpolarized surface. For resonant ionization rates $> 10^{14}$ s^{-1} and observation times in the range $10-50$ fs, indicated by the shaded area in Fig. 6.3, it is expected that the A_T/A_S ratio is rather insensitive to the exact resonant ionization rates and observation times. Experimentally we observed that indeed the A_T/A_S ratio depends only weakly on the observation time (thus on the perpendicular energy of the ion), as shown in Fig. 6.4. The three spectra from Fig. 6.4, taken at different kinetic energies of the He^{2+} ions (therefore the observation times are different), are very similar.

In order to incorporate explicitly the (possible) spin polarization of the sur-

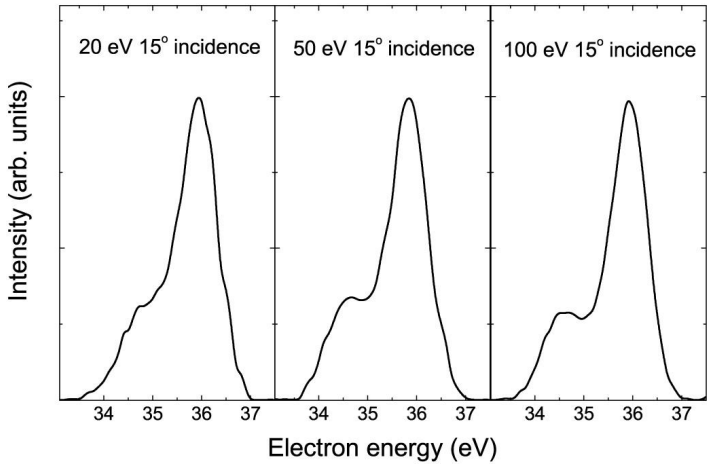

Figure 6.4: *Normalized KLL Auger electron spectra from He^{2+} ions incident on Ni(110) for a crystal temperature of 650 K.*

face electrons, the statistical population of the initial states is written as

$$g_i = (2L+1) \cdot \mathrm{P}_{\mathrm{spin}} \tag{6.3}$$

where $\mathrm{P}_{\mathrm{spin}}$ is the probability of populating a specific spin system (triplet or singlet) when capturing two electrons. If we write the spin polarization of the surface as

$$P = \frac{n_\uparrow - n_\downarrow}{n_\uparrow + n_\downarrow} \tag{6.4}$$

with $n_\uparrow$ and $n_\downarrow$ the fractions of spin-up and spin-down electrons, respectively ($n_\uparrow + n_\downarrow = 1$), then the probabilities to capture two electrons into either a triplet or a singlet state are

$$\begin{aligned} \mathrm{P_t} &= n_\uparrow n_\uparrow + n_\downarrow n_\downarrow + n_\uparrow n_\downarrow \\ \mathrm{P_s} &= n_\uparrow n_\downarrow \end{aligned} \tag{6.5}$$

From Eq. 6.4 and Eq. 6.5 it follows that

$$\begin{aligned} \mathrm{P_t} &= \frac{3+P^2}{4} \\ \mathrm{P_s} &= \frac{1-P^2}{4} \end{aligned} \tag{6.6}$$

For zero polarization one finds the statistical $3 \div 1$ ratio between triplet and singlet states. With the above ingredients KLL Auger spectra from He^{**} can be

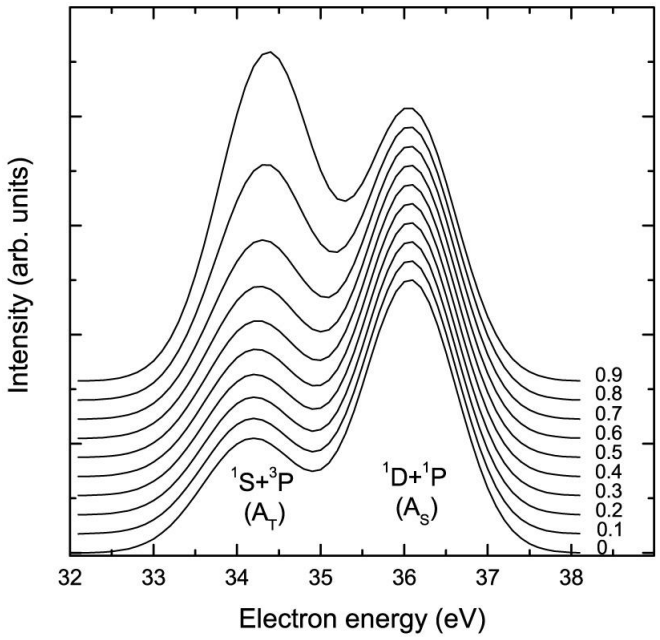

Figure 6.5: *Calculated spectra for 20 eV He^{2+} on Ni(110) under 15° incidence, for different degrees of polarization of the target, indicated on the right. The spectra are normalized to the higher energy (singlet) peak.*

simulated using a Monte Carlo method in the following manner: we include the statistical population of states from Eq. 6.3 and Eq. 6.6 in the expression for the fractions decaying by AI (Eq. 6.2). Then the atoms are allowed to decay along their trajectory by emitting an Auger electron at any random distance z between the neutralization distance z_{neut} and a distance above the surface where the quenching of the atomic states takes place ($\approx$ 2 a.u.). The energy of the emitted electrons will depend on z, as the difference between the initial and final state potential curves is dependent on z. The resulting energy distribution of the electrons is then convoluted with a Gaussian spectrometer function (FWHM=0.75 eV). A series of calculated spectra is shown in Fig. 6.5 for 20 eV He^{2+} impinging on a Ni(110) surface under 15° incidence, for different degrees of surface spin polarization (a constant offset has been added to the spectra, for clarity). The evolution of the calculated spectra is very similar to that of the measured ones shown in Fig. 6.6. The energy of the Auger peaks shifts to higher energies compared to the case of emission from atoms in the gas phase (from $\simeq$33.5 eV to $\simeq$34.4 eV for the triplet peak, and from $\simeq$35.4 eV to $\simeq$36 eV for the singlet peak), while the spacing between the peaks decreases. This result reproduces quite well

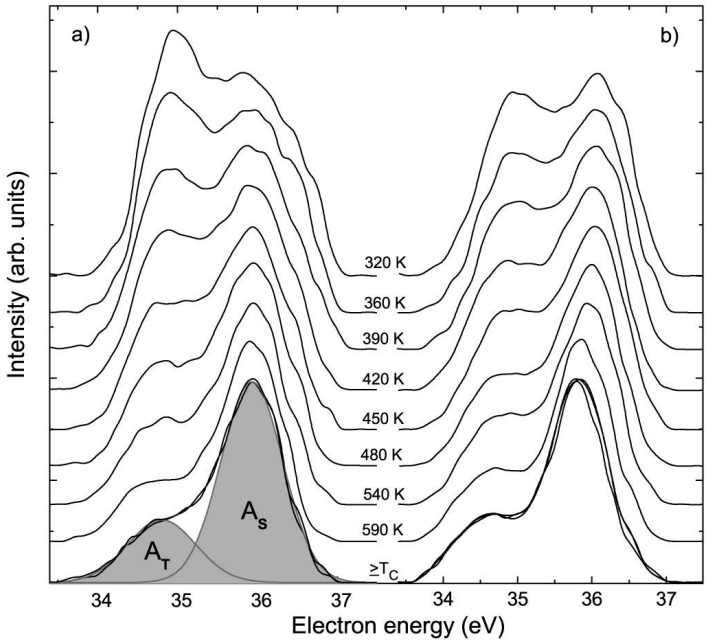

Figure 6.6: *KLL Auger electron spectra for a) 20 eV and b) 50 eV He^{2+} ions impinging on Ni(110) under 15° incidence, for different temperatures of the target. At T_C a two-Gaussian fit to the spectra is shown in grey.*

the peak shifts observed experimentally ($\simeq$34.6 eV for the triplet peak and $\simeq$36 eV for the singlet peak).

The intensity ratio of the triplet and singlet peak in the KLL spectra depends on the surface spin polarization and can be expressed as follows:

$$\frac{A_T}{A_S} = \frac{I_{^1\mathrm{S}} + I_{^3\mathrm{P}}}{I_{^1\mathrm{D}} + I_{^1\mathrm{P}}} = c_S + c_T \cdot \frac{3 + P^2}{1 - P^2} \tag{6.7}$$

with the coefficients c_S and c_T given by:

$$\begin{aligned} c_S &= \frac{I_{^1\mathrm{S}}}{I_{^1\mathrm{D}} + I_{^1\mathrm{P}}}\Big|_{P=0} \\ 3\,c_T &= \frac{I_{^3\mathrm{P}}}{I_{^1\mathrm{D}} + I_{^1\mathrm{P}}}\Big|_{P=0} \end{aligned} \tag{6.8}$$

The sum of c_S and $3c_T$ gives the triplet-to-singlet ratio for an unpolarized surface, in our case for temperatures of the crystal above Curie temperature T_C:

$$\frac{A_T}{A_S}\Big|_{T \geq T_C} = c_S + 3\,c_T \tag{6.9}$$

The numerical values fall in the interval $0.34 - 0.39$, for the observation times of our experiments. These values for the A_T / A_S ratio are very close to the ones we observed experimentally (between 0.33 and 0.4). As the spin polarization of the surface increases, so does the probability of capturing two electrons into triplet states, leading to an increase in the relative intensity of the triplet peak. Therefore, the triplet-to-singlet peak ratio can be used as a measure of the surface spin polarization.

6.2 Spin polarization of Ni(110)

The exchange interaction in a magnetic surface is weakened by the loss of magnetic neighbours, leading to a faster thermal decrease of the spin order. In models treating the temperature dependence of the surface spin polarization [95], two temperature ranges are described separately: the critical limit, i.e., temperatures close to the Curie temperature T_C, and the low temperature limit. For temperatures well below T_C, $T < 0.5 T_C$, in the regime of spin-wave models, the surface magnetization is expected to follow, like the bulk, the Bloch law $(1 - b\,T^{3/2})$, but with the coefficient b enhanced 2 to 3 times for the surface as compared to bulk [96, 97]. The critical behaviour near T_C is governed by a $(1 - T / T_C)^{\beta}$ law, with the critical exponent $\beta \simeq 0.7 - 0.8$ for surfaces, as compared to $\beta = 1/3$ for bulk ferromagnets [98].

6.2.1 Temperature dependence of the Ni(110) surface spin polarization

Knowing the A_T / A_S peak ratio for every temperature point and calculating c_S and c_T for every specific ion energy, Eq. 6.7 can be solved for P. In this way, the temperature dependence of the spin polarization can be determined. The results of this procedure are shown in Fig. 6.7. As the peak ratio has a quadratic dependence on the surface spin polarization (Eq. 6.7), the sign of the polarization needs to be determined independently. We used ECS on magnetized Ni(110) [25], and found a negative surface spin polarization for Ni(110). For all three projectile energies, two regimes can be clearly identified in the polarization temperature dependency. In the temperature range close to T_C, the polarization seems to follow a critical behaviour with the exponents β listed in Table 6.2. The values of β we obtained are reasonably close to $\beta = 0.76 \pm 0.02$ determined from SPLEED measurements, with high temperature resolution, by Alvarado *et al.* [99]. For temperatures lower than $0.7\,T_C$, a different dependency is evident. Although the temperature range of our measurements does not extend to temperatures low enough for the Bloch law behaviour to be fully valid, we attempted to fit a $T^{3/2}$ law to the surface polarization in the range $0.5 - 0.7\,T_C$, as shown by the solid

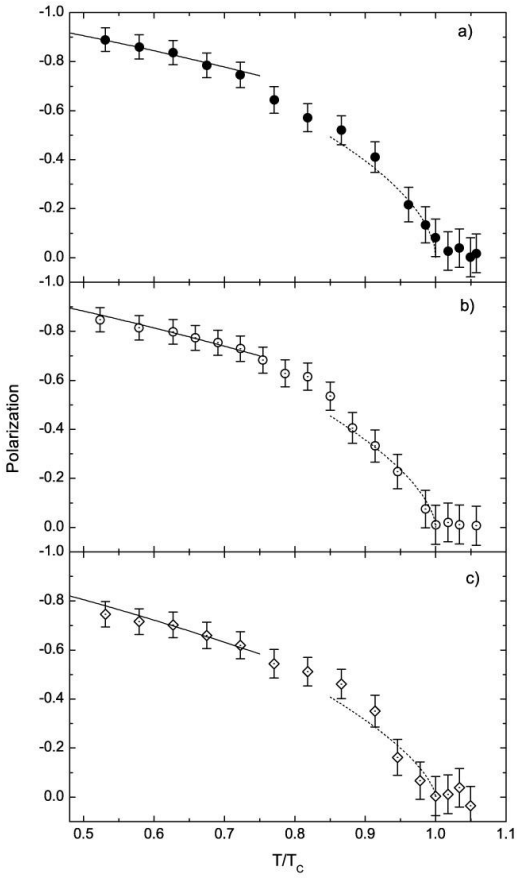

Figure 6.7: *Dependence of the surface spin polarization on the Ni(110) temperature, for: a) 20 eV, b) 50 eV, and c) 100 eV, 15° incidence He^{2+} ions. The solid curves are fits with a $(1 - b\,T^{3/2})$ dependence. The dashed curves are fits with a $(1 - T/T_C)^{\beta}$ dependence.*

Table 6.2: *Critical exponents and b-coefficients from fits to $P(T)$ of Fig. 6.7*

He^{2+} energy	β	$b\,[10^{-5}\,K^{-1}]$	b/b_{bulk}
20 eV	0.61 ± 0.14	1.9 ± 0.5	2.5
50 eV	0.65 ± 0.11	2.1 ± 0.4	2.8
100 eV	0.69 ± 0.15	2.3 ± 0.5	3

lines in Fig. 6.7. The coefficients *b* obtained from this fit are given in Table 6.2. These values are approximately three times larger than the one measured for bulk Ni, i.e. $7.5 \cdot 10^{-6}$ K$^{-3/2}$ [100], in accordance with the expected enhancement at the surface.

At room temperature ($\simeq 0.5\, T/T_C$), the polarization as obtained with 20 eV, 15° incidence He^{2+} ions is close to −90%, in agreement with previous theoretical and experimental results [69, 87]. We have to point out that this MECS value is the spin polarization of the electrons close to the Fermi level, as they are the ones (resonantly) captured into atomic levels. Other techniques for probing the spin polarization (like spin-polarized metastable de-excitation spectroscopy [77] or field emission electron spectroscopy [101]) deal with the polarization of electrons coming from a wider part of the band structure and the obtained values of the polarization are then different. Furthermore, in these latter cases electron tunnelling is involved and the (very) different tunnelling probabilities for *s* and *p*, on the one hand, and *d* electrons, on the other hand, have to be considered.

6.2.2 Spatial effects with MECS

Apparently, for 50 and 100 eV, 15° incidence He^{2+} ions, the polarization obtained at room temperature is lower than for 20 eV (cf. Fig. 6.7). The lower spin polarization observed for 50 eV and 100 eV He^{2+} ions hints at a weaker spin coupling of the captured electrons. The changes in the observed polarization are not likely to be caused by a variation of the electron polarization perpendicular to the surface, as trajectory simulations using the Kalypso 2 code [31] indicated that the turning point of the ions trajectory is the same for all ion energies used here (about 2 a.u. above the surface). The lowering of the polarization with increasing projectile energy can be understood if we bear in mind that the spin

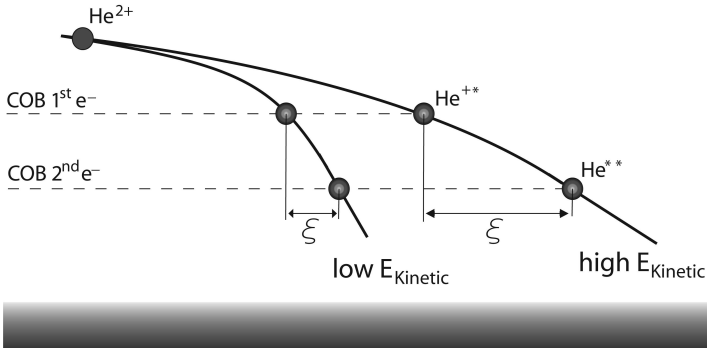

Figure 6.8: *Schematic depiction of trajectory effects induced by the charge-image charge interaction.*

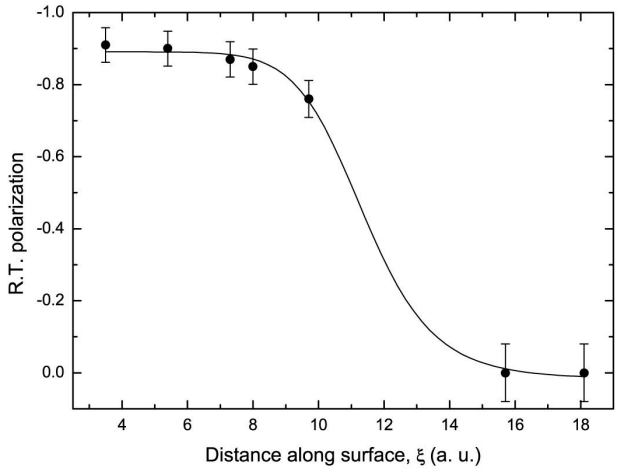

Figure 6.9: *Room temperature (R.T.) polarization of Ni(110) from MECS as function of the distance along the surface between the first and the second electron capture (according to COB model).*

correlation length[1] in Ni is in the order of $\simeq$ 20 a.u. [102,103]. According to COB, the distance along the surface between the first and the second electron capture for He^{2+} ions varies from $\sim$ 3 a.u. for 20 eV, 15° incidence to $\sim$ 10 a.u. for 100 eV, 15 ° incidence. The difference in distances along the surface is mainly caused by the image-charge interaction, which causes an energy gain perpendicular to the surface of $\approx$ 3 eV for He^{2+}. This leads to a larger effective incidence angle of the projectile. The lower the energy of the ion is, the larger the effective angle, because of the increased relative importance of the image-charge energy gain. This effect is schematically depicted in Fig. 6.8.

Fig. 6.9 shows the room-temperature (R.T.) polarization, obtained by MECS, as function of the distance along the surface between the first and the second electron capture, ξ. The data points were obtained from results using different He^{2+} energies and incidence angles (the solid curve is to guide the eye). Knowing the He^{2+} energy and the incidence angle, the distance ξ could be derived. The measured R.T. polarization shows a decreasing trend with increasing ξ, and, most striking, for grazing incidence the polarization vanishes. The distance along the surface between the first and the second electron capture is, of course, a crude approximation of the effective area from which the He^{2+} ions capture electrons. Nevertheless, Fig. 6.9 can give a fair idea of the scale of the spin correlation length, which seems to be about 12 a.u., if we take the value

[1] In a spin system at temperature T, the probability that two spins separated at distance r have the same orientation varies as $e^{-r/\xi}$, where ξ is the correlation length.

at the inflection of the $P(\xi)$ curve. Furthermore, it is of interest to investigate temperature-dependent $P(\xi)$ curves, which would allow to obtain the correlation length evolution with temperature.

6.2.3 Total intensity change in KLL Auger spectra from He**

So far we have focused on the changes in the relative intensities of the triplet peak, the advantage of using the A_T / A_S as measured quantity is the cancellation of possible long-term fluctuations in the ion beam current (due to thermal drifts and plasma instabilities in the ion source). The intensity of the singlet peak should decrease with increasing surface polarization (thus with decreasing surface temperature), as the weight of the capture probability shifts to the ^{3}P state. This implies that the total intensity of the emitted auto-ionization electrons should decrease with increasing surface spin polarization, because, as the capture in the ^{3}P state becomes more important, so does the electron loss via resonant ionization (due to the smaller branching ratio $\Gamma_{AI}^{^3\mathrm{P}} / (\Gamma_{AI}^{^3\mathrm{P}} + \Gamma_{RI})$ of the ^{3}P state compared to the singlet states).

These effects are illustrated in Fig. 6.10, in which the same series of spectra as

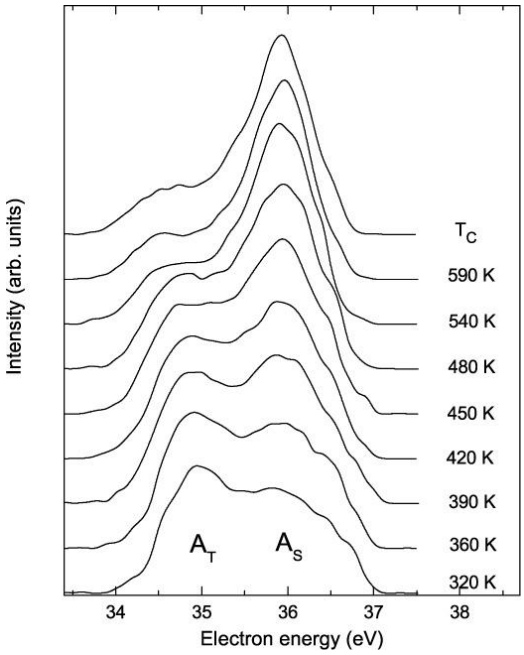

Figure 6.10: *Not normalized KLL Auger electron spectra from 20 eV He^{2+} on Ni(110) under 15° incidence (a constant offset is added for clarity).*

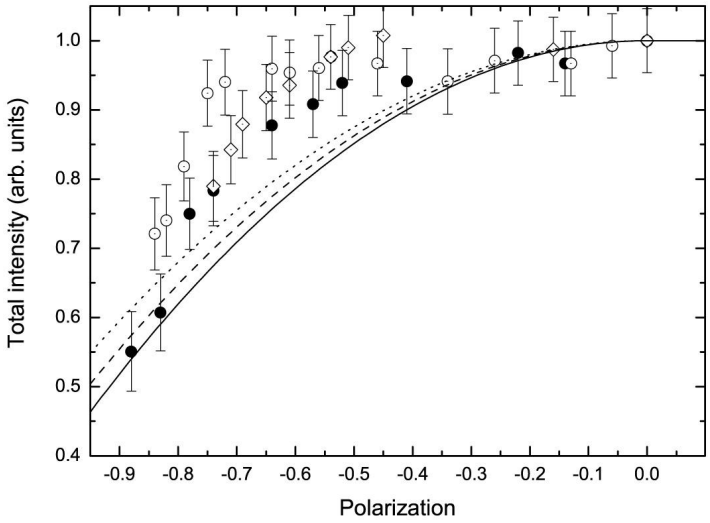

Figure 6.11: *Polarization dependency of the total intensity of auto-ionization electrons from 20 eV (●), 50 eV (○) and 100 eV (◇), 15° incidence He^{2+} ions on Ni(110). The curves are the calculated intensities for 20 eV (solid line), 50 eV (dashed line), and 100 eV (dotted line) He^{2+} ions.*

in Fig. 5.3 is shown, but this time not normalized. In Fig. 6.10 it can be seen that the decrease of the triplet peak is concurrent with the increase of the singlet peak, as the temperature of the Ni(110) crystal increases. By integrating the spectra over the whole energy range of interest, the total intensity is obtained. Using the polarization dependencies on temperature (Fig. 6.7), the total intensity can be plotted as a function of the surface polarization. This is shown in Fig. 6.11. The curves are the calculated total intensities from the free-atom model, for the three projectile energies that we have used. All series have been normalized to the intensity value at T_C, which corresponds to zero polarization.

For each of the three scattering conditions, the calculated total intensity dependence on polarization was obtained by summing the decayed fractions corresponding to the four states contributing to the KLL Auger spectra. The atomic model describes the data fairly well. As points of improvement, the variation of the decay rates with the ion-surface distance should be included in the model, as they are strongly influencing the total electron emission. However, the problem of Auger transition rates in front of metallic surfaces is not straightforward, and accurate theoretical and / or experimental data are needed. Wethekam *et al.* [104] obtained promising results on the Auger neutralization of He^+ ions in front of metallic surfaces. When considering peak intensity ratios though, it is reasonable to assume that the changes in the auto-ionization rates follow the same be-

haviour for the four $(2l2l')$ states in He** and therefore cancel out. Another point of improvement in the model could be the inclusion of the possibly different emission anisotropies of the $(2l2l')$ states in doubly-excited He, or taking into consideration the Auger de-excitation process which becomes the dominant decay channel for close ion-surface distances.

Conclusions

Using an atomic model based on concepts from the COB model [16], the changes observed in the KLL Auger electron emission from He** could be quantitatively related to the surface spin polarization of the Ni(110) surface. The temperature dependence of the Ni(110) spin polarization follows a behaviour expected for typical ferromagnetic surfaces [96–98]. Changes in the observed polarization as function of the distance along the surface travelled by the projectile indicate that MECS could provide information on the magnetic characteristics on a (sub)-nanometer scale.